https://doi.org/10.5194/egusphere-2026-5113
Preprint. Discussion started: 4 September 2026

Accounting for surface reflectance variations along the satellite line of sight for UV-Vis ozone limb retrievals.

Carlo Arosio[1], Alexei Rozanov[1], Vladimir Rozanov[2], Andrea Orfanoz-Cheuquelaf[3], John P. Burrows[1], Edward Malina[4], and Hartmut Boesch[1]

[1]Institute of Environmental Physics, University of Bremen, Bremen, Germany
[2]Institute of Environmental Physics, University of Bremen (Retired), Bremen, Germany
[3]Max-Plank-Insitute for Meteorology, Hamburg, Germany
[4]European Space Agency, ESRIN, Frascati, Italy

Correspondence: Carlo Arosio (carloarosio@iup.physik.uni-bremen.de)

Abstract. Retrievals of stratospheric ozone profiles from space-borne limb-scatter measurements in the UV-Visible spectral range were found to produce a bias if the effective reflectance of the underlying scene has a strong gradient along the instrument line of sight. This effect is particularly pronounced when the underlying scene between the sub-satellite and the tangent point passes from desert to ocean or from cloudy to cloud-free conditions, especially over the ocean. For stratospheric ozone columns retrieved from Ozone Mapper and Profiler Suite Limb Profiler (OMPS-LP) observations, regional biases of up to 7-10 DU were detected. When applying the limb-nadir matching technique, i.e. combining stratospheric and total ozone column information to obtain the residual tropospheric column, these underlying scene related biases amount to about 10-30 % of typical tropospheric ozone column values.

In this manuscript we present an improved retrieval algorithm, which substantially mitigates the observed biases in the stratospheric and tropospheric ozone. The algorithm employs an extended version of the SCIATRAN radiative transfer model (v4.8) capable of accounting for variations of the effective reflectance of the underlying scene along the instrument line of sight. VIIRS observations are used to prescribe the variation of the effective reflectance of the underlying scene along the instrument line of sight in the radiative transfer model. The manuscript describes the implementation strategy, discusses the results in terms of stratospheric ozone changes with respect to the standard version and presents updated OMPS-LP/OMPS-NM and new OMPS-LP/TROPOMI tropospheric ozone column datasets along with the validation of the results with respect to correlative observations. Any retrieval of observations from solar limb sounding spectrometers is potentially affected by this issue and should take it into account.

1 Introduction

While stratospheric ozone protects mankind from harmful UV radiation, and plays an essential role in the thermal balance and dynamics of the stratosphere, tropospheric ozone is a major pollutant, which is detrimental to human health, and an important greenhouse gas. Tropospheric ozone is produced by the interaction between nitrogen oxides and hydrocarbons in the presence of sunlight (Crutzen et al., 1999) and can reach concentrations, which are harmful for human health and crops, especially

https://doi.org/10.5194/egusphere-2026-5113
Preprint. Discussion started: 4 September 2026

during intense summer smog episodes. Damages to ecosystems by ozone pollution are related to water acidification, leading to yield losses and damages of crops and forests. Tropospheric ozone contributes to the anthropogenic greenhouse effect with a radiative forcing of $0.40 \pm 0.20\ \mathrm{W\,m^{-2}}$ (Stevenson et al., 2013).

Global scale information on short- and long-term variations of tropospheric ozone can only be obtained from observations by space-borne instruments. Beside the tropospheric ozone retrievals from nadir ozone profiles, e.g. (Keppens et al., 2024), from cloud slicing, e.g. (Ziemke et al., 2005) and convective cloud differential methods, e.g. (Heue et al., 2016; Leventidou et al., 2016), tropospheric ozone can be provided by using the limb-nadir matching (LNM) technique applied to a combination of space borne observations in limb and nadir viewing geometries. A similar approach can also be applied to combined simultaneous measurements of nadir UV-Vis and thermal infrared observations (Mettig et al. (2022) and references therein). At the University of Bremen, Institute of Environmental Physics (IUP), an algorithm to retrieve tropospheric ozone columns by applying the LNM technique to observations from the Suomi-National Polar Partnership (SNPP) Ozone Mapper and Profiler Suite (OMPS) has been developed (Orfanoz-Cheuquelaf et al., 2024). Tropospheric ozone columns (TrOC) are obtained by subtracting the stratospheric ozone columns (SOC), which are retrieved from OMPS-Limb Profiler (LP) measurements (Arosio et al., 2018), from the total ozone columns (TOC) obtained from coinciding OMPS-Nadir Mapper (NM) observations (Orfanoz-Cheuquelaf et al., 2021). Both SOC and TOC retrieval algorithms were previously developed at IUP, based on the SCIATRAN radiative transfer model (RTM) and retrieval software, which assumed a 1-D atmosphere, i.e. atmospheric layers and underlying surface were considered to be horizontally homogeneous along the instrument line of sight (LOS). Of historical note, the use of near simultaneous measurement of scattered solar radiation for the retrieval of trace tropospheric gases was first proposed for the SCIAMACHY project (Burrows et al. (1995) and references therein).

Orfanoz-Cheuquelaf et al. (2024) identified the presence of regional artifacts in the retrieved LNM dataset, particularly in the tropical Pacific region. This is illustrated in Fig. 1, which shows a multi-year average map of tropospheric ozone global anomalies, where a positive band-shaped artifact across the Pacific ocean is observed a few degrees north of the equator. Similar artifacts were also found in other TrOC products derived from space-borne measurements in the UV-Vis spectral range, e.g. in the SCIAMACHY LNM dataset (Orfanoz-Cheuquelaf et al., 2024). As discussed in more detail in Sect. 2, this artifact originates from the limb SOC and is caused by the presence of the Inter-Tropical Convergence Zone (ITCZ) (Hwang and Frierson, 2013). Within the ITCZ, a semi-permanent continuous cloud band develops a few degrees north of the equator. This bright cloud band extends roughly perpendicularly to the viewing direction of the OMPS-LP instrument and is surrounded in the south-north direction by the ocean surface with typically low reflectance. Along any instrument LOS crossing this area, strong gradients in the upwelling tropospheric radiance occur, which cannot be accounted for by using standard (1D) RTMs and cause retrieval artifacts. Due to the semi-stationary nature of the ITCZ over the Pacific, this feature is not averaged out and is evident in the multi-year average maps.

The physical origin of this artifact is related to the limb viewing geometry: for such observations, a substantial amount of light entering the instrument field-of-view (FOV) is reflected by the Earth's surface or scattered within the boundary layer or clouds (Oikarinen and Kyrölä, 1999). As discussed by Oikarinen (2002), the reflection from a region about $\pm 75\ \mathrm{km}$ across-track and $\pm 500\ \mathrm{km}$ along-track around the tangent point (TP) constitutes about 95 % of the total reflected intensity received

https://doi.org/10.5194/egusphere-2026-5113
Preprint. Discussion started: 4 September 2026

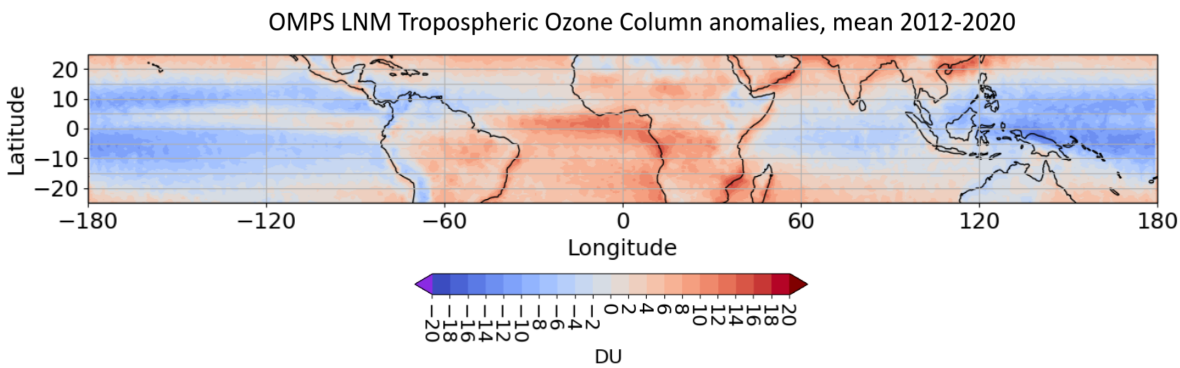

Figure 1. TrOC global anomalies from LNM OMPS data, averaged over 2012-2020.

by the instrument. The study highlighted a potential need for modeling the reflected intensity using surface albedo data from concurrent measurements by other instruments. In fact, although in typical UV-Vis limb retrievals the effects of the underlying scene reflectance are mitigated by normalizing the measured data by a reference spectrum observed at a high tangent altitude (Flittner et al., 2000), the retrieval results are still significantly dependent on the method to account for the reflectance of the underlying scene. This is especially the case for space borne instruments which register a full vertical image at once (such as OMPS-LP) because every tangent point of the limb image has somewhat different geographic location.

Typically, limb-scatter retrievals are performed assuming a horizontally homogeneous effective Lambertian surface albedo in the forward model. However, on a scale of several hundred kilometers, the reflectance of the underlying scene can vary substantially. The most complicated scenario, which is relevant for our investigation, is when the distribution of the underlying scene reflectance is not symmetric with respect to the TP and shows a strong gradient in the reflectance occurring between the tangent point and the instrument (near field).

Several retrieval approaches accounting for the inhomogeneity of the atmosphere along the instrument LOS have been developed during the last decades for limb-emission, e.g. Steck et al. (2005); Livesey et al. (2006), and limb-scatter retrievals (Zawada et al., 2018). However, these approaches are focused on accounting for variations in the ozone amount rather than the reflectance properties of the atmosphere or underlying surface. In this manuscript, we present a new retrieval approach, which uses the effective Lambertian surface albedo measured by the VIIRS instruments to initialize the SCIATRAN RTM. The latter has been extended to account for variations of the effective surface albedo along the instrument LOS, including clouds.

The paper is structured as follows: in Section 2 the space-borne instruments and their datasets used in the study are presented. In Section 3 the ozone retrieval and known artifacts are discussed. Section 4 describes the modifications implemented in the SCIATRAN RTM and the usage of an external surface albedo dataset. In Section 5 the surface spectral reflectance or albedo datasets are presented. Section 6 introduces the resulting stratospheric profiles obtained with the newly developed retrieval approach and compares them with correlative data. Finally, Sect. 7 introduces the LNM datasets which were created using the updated stratospheric information and validates the results against ozonesonde data.

https://doi.org/10.5194/egusphere-2026-5113
Preprint. Discussion started: 4 September 2026

2 Used data

Most of the data used in this study are derived from OMPS measurements; the instrument was launched in October 2011 on board the SNPP satellite platform, started measuring in February 2012 and is still in operation. OMPS comprises a suite of three instruments: two nadir-looking, the Nadir Mapper (OMPS-NM) and the Nadir Profiler (OMPS-NP), and OMPS-LP performing limb observations. As mentioned above, retrievals of the ozone total column from OMPS-NM and of the stratospheric ozone profiles from OMPS-LP have been developed at IUP Bremen over the last decade (Arosio et al., 2018; Orfanoz-Cheuquelaf et al., 2021). The datasets from these retrievals are used in this study.

OMPS-NM is a spectrometer measuring back-scatter solar radiation in the UV spectral range from 300 to 380 nm, with a spectral resolution of 1 nm (Flynn et al., 2014). The footprint of OMPS-NM is approximately 50 x 2800 km^2, with a field of view (FOV) of 0.27° ($\sim$ 50 km) along-track and 110° across-track swath, divided into 36 bins (ground pixels). The across-track FOV naturally increases towards the edges of the swath, with a 20 km to 50 km FOV for the near-central pixels.

The OMPS-LP instrument observes the atmospheric limb in the backward direction through three vertical slits, from which the well calibrated measurements of the central one pointing along the satellite's orbital plane are used in this study. The central slit is designed to observe the same air masses as in the nadir viewing geometry about 7 min later. Observations are performed in the ascending node with the equator crossing time of 13:30. OMPS-LP performs 180 observations per orbit from which around 140 are at solar zenith angles smaller than 80°. Horizontal sampling is about 3 km across track and 200 km along track. The spectral coverage of OMPS-LP ranges from the UV (280 nm) to the NIR (1020 nm). A 2D CCD detector observes the atmosphere from the surface to 100 km having a vertical sampling of 1 km. The vertical field of view is about 1.5 km for each detector pixel.

One of the LNM products presented in this manuscript uses observations form the TROPOspheric Monitoring Instrument (TROPOMI), which was launched on board the Copernicus Sentinel-5 Precursor (S5P) satellite in October 2017, with data available from May 2018, and is still in operation (Veefkind et al., 2012, 2018). TROPOMI has an ascending node equatorial crossing time of 13:30, a ground pixel size of 3.5 km x 7 km for TOCs and all major atmospheric gases retrieved from the UV-Vis, a swath of 2600 km, and daily global coverage with about 14 orbits per day.

As explained in Sect. 4, in the improved retrieval algorithm we use surface albedo information extracted from the Visible Infrared Imaging Radiometer Suite (VIIRS) dataset (Cao et al., 2013). The VIIRS instrument is also onboard the SNPP satellite platform and observes the radiance upwelling from the Earth's atmosphere across visible, near-infrared, and shortwave infrared wavelengths, covering the spectral range from approximately 410 nm to 2250 nm. For our study, we used surface reflectance values in the visible band at 673 nm, which we consider representative for the Chappius band, given that ocean reflectance and cloud albedo have a small wavelength dependence across the visible range.

3 Standard ozone retrieval and identified retrieval artifact

The SCIATRAN RTM (Rozanov et al., 2014) is used as the forward model in the stratospheric ozone profile retrieval algorithm developed over the past three decades at the IUP Bremen to simulate the radiance scattered by the Earth's atmosphere and

https://doi.org/10.5194/egusphere-2026-5113
Preprint. Discussion started: 4 September 2026

reflected by the surface. The retrieval employs a standard iterative procedure (Arosio et al., 2018): first the SCIATRAN forward model is used to simulate the measured spectrum and Jacobians for a first guess ozone profile, then, the ozone profile is retrieved based on the difference between the simulated and measured radiances and regularization constraints, the result is used to initialize the forward model for the next run. The iterative process is stopped when the difference between two subsequent solutions in the selected altitude range does not exceed a chosen criterion. The regularization employs a first order Tikhonov constraint. Four spectral segments are selected to retrieve ozone from OMPS-LP observations: three in the UV region and one in the Chappuis band, see Arosio et al. (2018, 2024). The altitude range over which the retrieval is performed spans from 8 to 60 km above sea level. Limb radiances in each spectral interval are normalized by a limb measurement at an upper tangent height (TH), in order to provide a self-calibration of the instrument and reduce the effect of surface-cloud reflectance. In the standard retrieval approach, the surface spectral reflectance reaching the OMPS field of view, also known as effective surface albedo, is assumed to be horizontally homogeneous. It is retrieved simultaneously with the ozone retrieval exploiting a sun normalized radiance spectrum measured at an upper tangent height. Beforehand, a cloud filter is applied rejecting measurements at tangent heights affected by clouds, and the aerosol retrieval is performed, whose results are used then in the forward model within the ozone retrieval.

3.1 Identified retrieval artifact

In this section, we describe the retrieval artifact identified in the stratospheric ozone columns resulting from the standard retrieval over the tropical Pacific region. Figure 2 shows the SOC, cloud top height and the effective Lambertian surface albedo retrieved from OMPS-LP measurements and averaged over the tropical Pacific region from July to September 2016. In addition, the SOC from the Microwave Limb Sounder (MLS) are displayed, which is used as a reference instrument in this study because it cannot suffer from the same effect. This instrument performs microwave emission measurements and is not affected by the described artifact because it is insensitive to the reflectance of the underlying scene.

The effective Lambertian surface albedo, which characterizes the reflectance of the underlying scene, was obtained from observations in the nadir-viewing geometry by the OMPS-NM instrument. It is seen from the figure that the OMPS-LP SOC shows a dip with respect to the MLS data with the largest discrepancies located around 5° N, a few degrees south of the maximum in the reflectance of the underlying scene and cloud top height. This dip corresponds to the positive anomaly artifact shown in Fig.1 (TrOC = TOC - SOC) and is caused by the presence of the highly reflecting cloud band located between the instrument and the TP (near field) below the field of view of the lowermost detector pixel (corresponding to the lowermost TH) used in the retrieval. On the contrary, the presence of the highly reflecting cloud band beyond the TP (far field) causes a positive bias in OMPS-LP SOC around 10-15 ° N. The latter is, however, significantly less pronounced.

4 Extension of the SCIATRAN RTM and a proof of concept analysis

To mitigate the artifact described above, the capability of the forward model used in the retrieval must be extended, to account for variations of the underlying scene reflectance along the instrument LOS. Although the latest standard version of SCIATRAN

https://doi.org/10.5194/egusphere-2026-5113
Preprint. Discussion started: 4 September 2026

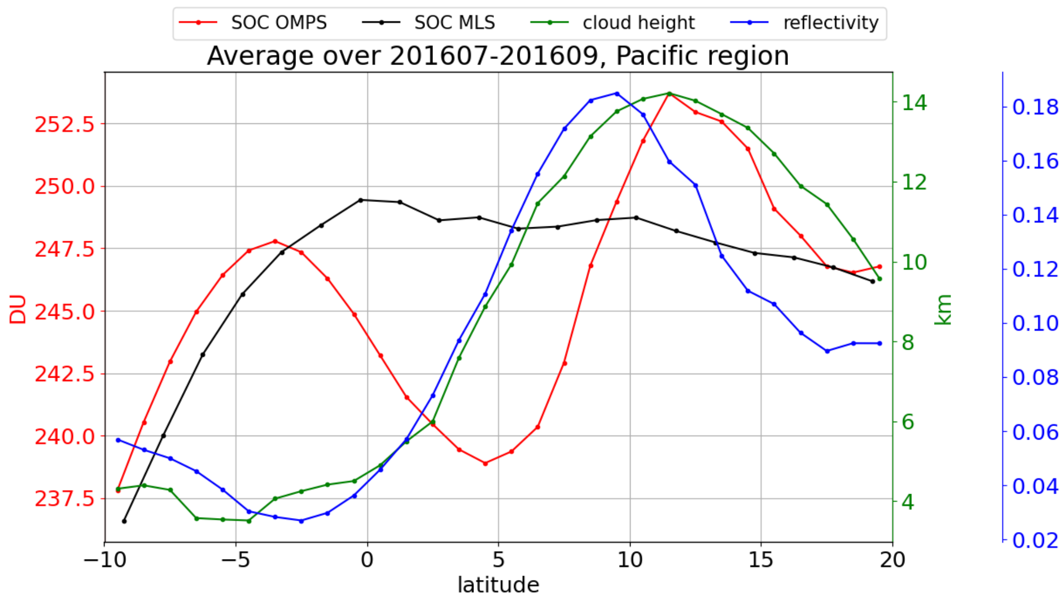

Figure 2. SOC and cloud top height from OMPS-LP (red and green, respectively), effective Lambertian surface albedo from OMPS-NM (blue), and SOC from MLS (black, which also uses the left red axis). All data are averaged over the Pacific sector from July to September 2016.

(v4.7) is capable of handling variations of trace gas absorption as a function of solar zenith angle, the scattering properties of the atmosphere and the reflective properties of the underlying surface are assumed horizontally homogeneous.

For this study, the reflectance of the underlying scene was represented by effective Lambertian surface albedo. The extension to SCIATRAN uses the so-called independent pixel approximation approach in the framework of the combined differential-integral (CDI) technique (Rozanov et al., 2001). In this approach, a fully spherical ray tracing is used to calculate the LOS coordinates and the contribution of the single scattering. To account for the multiple scattering contribution, the radiation field is calculated at a selected grid along the instrument LOS employing the pseudo-spherical approximation (spherical ray tracing for the direct solar beam and the plane-parallel treatment for scattering processes) and then integrated along the LOS intersecting the spherical atmosphere. The only difference between the new version of SCIATRAN and the standard version is that the latter uses the solar zenith angle grid to calculate the pseudo-spherical multiple scattering radiation field while the new extended version uses a grid of geographical locations along the instrument LOS and the Lambertian surface albedo can be specified at each grid point, independently based on its geographical coordinates. The SCIATRAN version capable of accounting for variations of the surface albedo is referred to as v4.8 and the retrievals performed using this version are referred to in the following text as 2D-mode retrievals. Figure 3 shows a schematic view of the retrieval chains for the 1D standard processing and for the 2D-mode; the surface albedo information is detailed in Sect. 5.

https://doi.org/10.5194/egusphere-2026-5113
Preprint. Discussion started: 4 September 2026

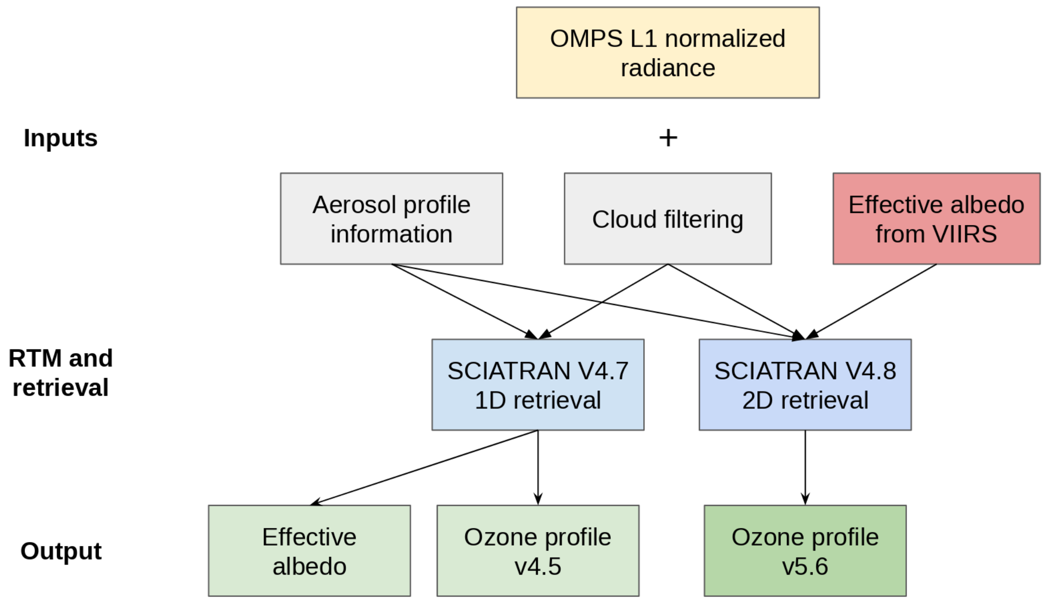

Figure 3. Schematic view of the 1D and 2D-mode retrieval chains.

An initial verification of the extended SCIATRAN RTM (v4.8) was achieved by testing the ability of synthetic retrievals to reproduce the observed artifact. To this end, we used the extended version of SCIATRAN to simulate the limb radiance for a sample surface albedo distribution in the Pacific characterized by a pronounced isolated pattern in the underlying scene reflectance. The simulations were performed for several TP locations, a few degrees South and North of the peak of the underlying scene reflectance. Then these simulated limb radiances were used as the input to the standard (1D) retrieval. For comparison, the retrieval was also performed for the limb radiance simulated with the standard SCIATRAN RTM (v4.7), the results of this retrieval are referred to as the unperturbed run. The results of these synthetic retrievals are illustrated in Fig. 4. We see that for the unperturbed run (green star), the profile resulting from the 1D retrieval coincides with the a-priori profile (and with the result from the 2D-mode retrieval, not shown). On the contrary, for the TPs located to the South of the reflectance peak (blueish colors), the 1D retrieval strongly underestimates the ozone number density, whereas for the TPs to the North of the peak (reddish colors) an overestimation is observed. These results reproduce the wave-like structure seen in Fig. 2. The effect is observed mostly below 32 km, where the Chappius band is used for the retrieval. The largest differences are found around the peak of the number density profile.

This example confirms that the identified artifact is caused by the inhomogeneity of the underlying scene reflectance along the instrument LOS, which cannot be properly accounted for within the 1D retrieval. We also investigated the dependence of the artifact on the cloud top height and on the magnitudes of the absolute value and of the gradient of the underlying scene reflectance. We found a direct correlation between the steepness of the gradient in the underlying scene reflectance and the magnitude of the artifact.

https://doi.org/10.5194/egusphere-2026-5113
Preprint. Discussion started: 4 September 2026

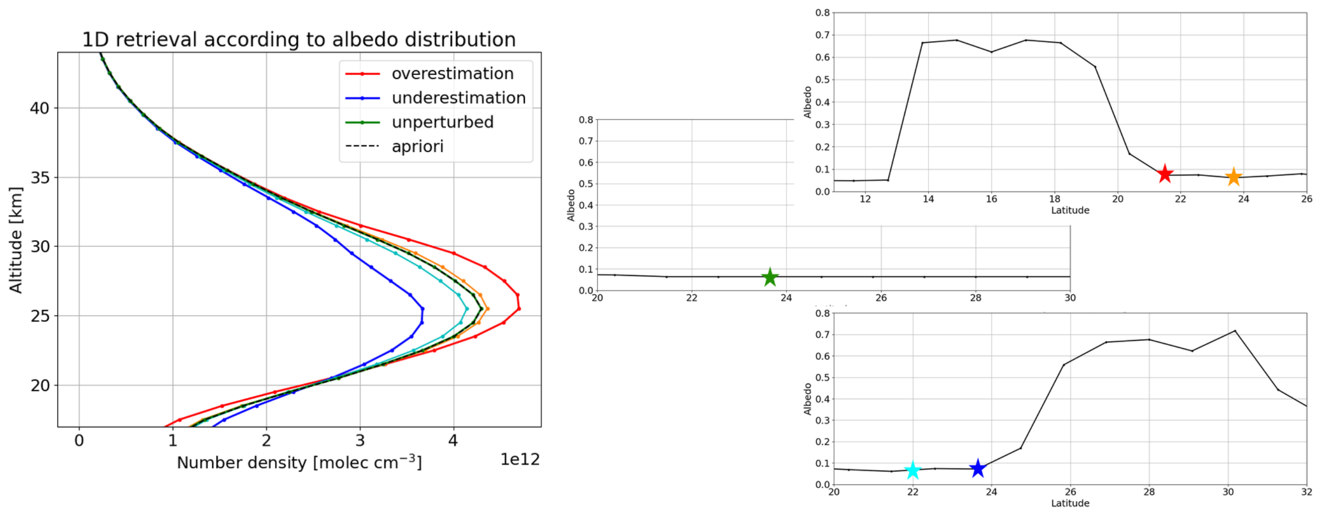

Figure 4. Results of the synthetic simulations for several TPs located a few degrees South and North of the underlying scene reflectance peak. The color of the stars in the right panels (TP locations) corresponds to that of the profiles in the left panel.

5 Surface albedo datasets

In order to initialize the 2D-mode retrieval, we need to prescribe the effective Lambertian surface albedo values along the orbit for each OMPS-LP observation. To this end, three candidate datasets were considered:

1. Data from the OMPS Nadir Mapper (NM), retrieved at IUP Bremen (Orfanoz-Cheuquelaf et al., 2021). This instrument was optimized to observe the scene which is observed 7 minutes later by the OMPS-LP instrument. Unfortunately, the wavelength range of the OMPS-NM instrument is restricted to UV, whereas the knowledge of the effective Lambertian surface albedo in the visible range is required for the 2D-mode retrieval. This is because the artifact affects ozone profiles mostly below 32 km, where the spectral information from the Chappuis absorption band of ozone is used.

2. Data from TROPOMI. The instrument provides daily maps of effective Lambertian surface albedo in the visible spectral range. However, TROPOMI was launched in 2017 and its dataset does not cover the entire OMPS mission, which started in 2012.

3. Data from VIIRS. The instrument is on board the same satellite platform as OMPS and its observations are nearly collocated with those from OMPS-LP. VIIRS dataset provides values of the effective Lambertian surface albedo in several spectral bands including the visible spectral region.

We compared the effective Lambertian surface albedo values retrieved simultaneously with ozone profiles by the standard IUP OMPS-LP algorithm, and the values provided in TROPOMI and VIIRS datasets. We found generally good agreement between the three zonally averaged datasets with a small difference between OMPS-LP results and TROPOMI/VIIRS data,

https://doi.org/10.5194/egusphere-2026-5113
Preprint. Discussion started: 4 September 2026

which increases towards northern high latitudes (see Supplements, Fig. S1). This discrepancy might produce a bias between the mean SOC values from 1D and 2D-mode retrievals, which increases in the Northern Hemisphere.

6 2D-mode retrieval results

6.1 SOC results for selected orbits

For the first tests on real data, we selected OMPS-LP orbits characterized by a strong isolated peak in the underlying scene reflectance along the orbit, i.e. two consecutive observations with high reflectance (in particular above 0.5) surrounded by observations with low reflectance (below 0.3) (an example in the Supplements Fig. S2). We found about 30 suitable orbits in 2019 located in different regions/latitudes. For these orbits, we run both the standard and the 2D-mode retrievals. For each orbit, the location of the maximum of the underlying scene reflectance gradient (Δ) was taken as a reference. Then, the SOC calculated for each observation around this location were sorted as a function of their distance from Δ. In Fig. 5, the difference between SOC from OMPS-LP and collocated MLS measurements is displayed as a function of the distance from Δ for the 1D (left panel) and the 2D-mode (right panel) retrievals.

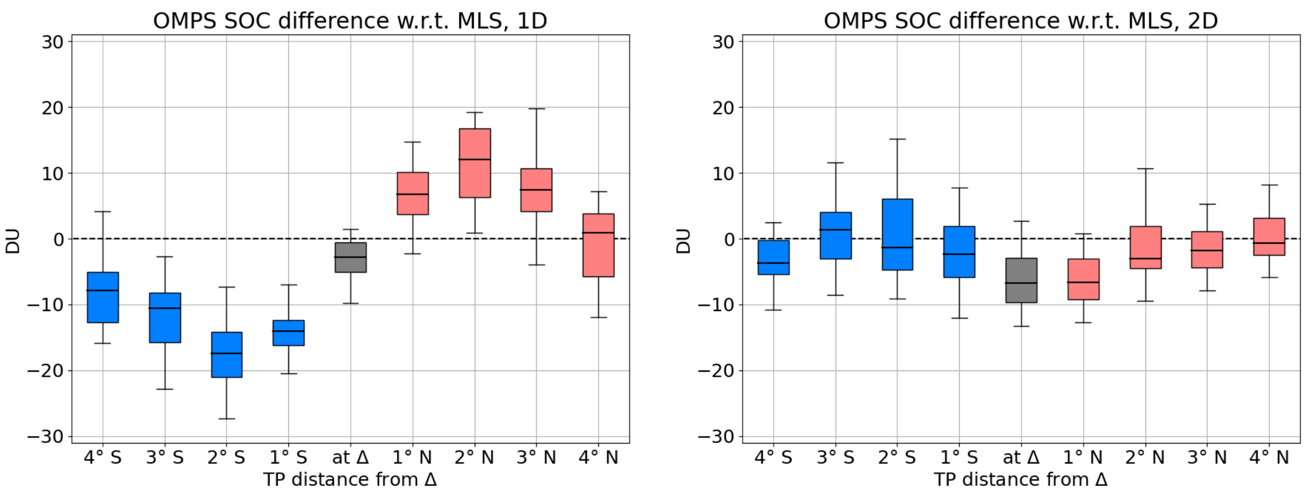

Figure 5. Difference between collocated OMPS-LP and MLS SOC averaged over 30 selected orbits as a function of the distance from the location of the maximum of the underlying scene reflectance gradient (Δ, gray box). Left panel: 1D retrieval, right panel: 2D-mode retrieval.

https://doi.org/10.5194/egusphere-2026-5113
Preprint. Discussion started: 4 September 2026

The typical wave-shaped artifact is pronounced for the 1D retrieval results, with OMPS-LP SOC underestimation occurring when the TP is located to the South of the sharp gradient in the underlying surface reflectance (maximum at 2° S) and overestimation occurring when the TP is located to the North of it. As it was already noticed in Fig. 2, the negative artifact is larger in absolute values than the positive one. This is related to the geometry of limb observations: the negative artifact occurs when the underlying scene reflectance gradient, e.g. a cloud, is located in the near field, i.e. between the satellite and the TP. In this case the inhomogeneity of the underlying scene reflectance has a larger impact on the retrieval. On the other hand, the positive artifact occurs when the reflectance gradient is located in the far field, i.e. to the South of the TP. Looking at the right panel of Fig. 5, we notice that for the 2D-mode retrieval the distribution of the difference with respect to MLS is significantly flatter, i.e. more independent from the location of the underlying scene reflectance gradient. In this case the SOC from OMPS-LP and MLS agree within the uncertainties (standard deviations of the differences).

6.2 Artefact mitigation in selected regions

A further evaluation of the 2D-mode retrieval results has been performed in selected regions of interest, where sharp gradients in the underlying scene reflectance along the OMPS-LP LOS are expected. For comparison we also performed retrievals using the effective Lambertian surface albedo from TROPOMI and using different griddings for the VIIRS albedo. Figure 6 shows the SOC retrieval results from OMPS-LP using different effective Lambertian surface albedo data as well as SOC from collocated MLS measurements for the Pacific sector and the Arabian Peninsula region. The data were averaged from July to September 2021. In panel (a), the SOC cross sections over the Arabian Peninsula are displayed. The values from MLS (black), OMPS-LP 1D (blue) and OMPS-LP 2D-mode, the latter using TROPOMI (magenta) and VIIRS (red) surface albedo data, are shown along with the effective surface albedo from VIIRS (green). The latter depicts the ocean-to-continent (desert) transition, which spreads roughly perpendicular to OMPS-LP orbit tracks. We clearly see the expected negative artifact in the 1D retrieval located a few degrees to the south from the effective surface albedo maximum. In contrast, the results from 2D-mode retrieval show good agreement with MLS results for both TROPOMI and VIIRS surface albedo datasets. In panel (b), similar to panel a), the SOC cross sections over the Pacific sector are shown, but here we compared OMPS-LP 2D-mode results using different griddings of the VIIRS surface albedo data rather than VIIRS/TROPOMI. We note that the red and the orange curves overlap. Again, we can identify the wave-shaped artifact in the 1D retrieval whereas the 2D-mode results show good consistency with the MLS SOC. When analyzing the effect of different sizes of the horizontal grid boxes used to average the VIIRS surface albedo data around each TP, we see that the results are very similar. For further investigations, we averaged VIIRS surface albedo data using the horizontal box size of $1° \times 1°$ and sampled them in 0.5° steps along the orbit to initialize the SCIATRAN model. These values provide an optimal trade-off to avoid outliers in the VIIRS data and still capture sharp surface albedo gradients.

https://doi.org/10.5194/egusphere-2026-5113
Preprint. Discussion started: 4 September 2026

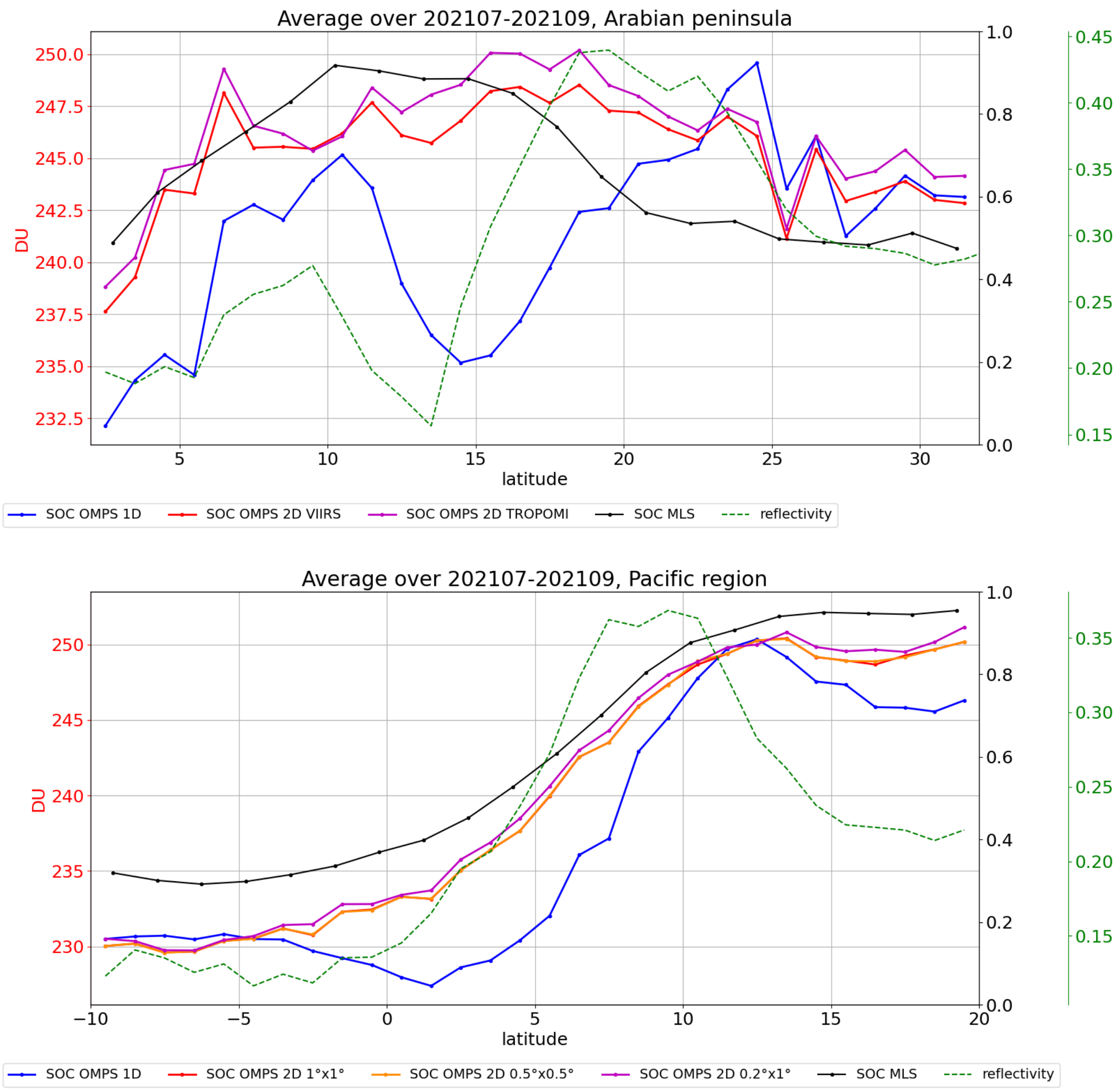

Figure 6. Cross sections of SOC from OMPS-LP and MLS over the Arabian Peninsula region (top panel) and over the Pacific sector (bottom panel). The OMPS-LP results are shown for 1D and 2D-mode retrievals. The latter results are shown for surface albedo datasets form VIIRS and TROPOMI (in panel a) and for different horizontal averaging of the VIIRS albedo (in panel b).

6.3 Data set validation against MLS and ozonesondes

In this section, we present validation results for the OMPS-LP dataset processed employing the 2D-mode approach, which is identified as v5.6. The OMPS-LP 1D dataset was also updated to have the same retrieval settings (e.g., aerosol extinction coef-

https://doi.org/10.5194/egusphere-2026-5113
Preprint. Discussion started: 4 September 2026

ficient, altitude normalization, cloud screening) as the 2D-mode dataset, and referred to as v4.5. As reference data, collocated measurements made by MLS and ozonesondes were used.

For each OMPS-LP observation, we selected a nearest-neighbor MLS v5 ozone profile with a maximum time difference of 6 hours and a maximum distance of 1° in latitude and 2° in longitude. The vertical resolution of the two products is comparable, about 2-3 km. The relative difference between the OMPS-LP profiles and collocated MLS results as a function of latitude and altitude, is shown in the left panel of Fig. 7 . The results were averaged over the entire year of 2016.

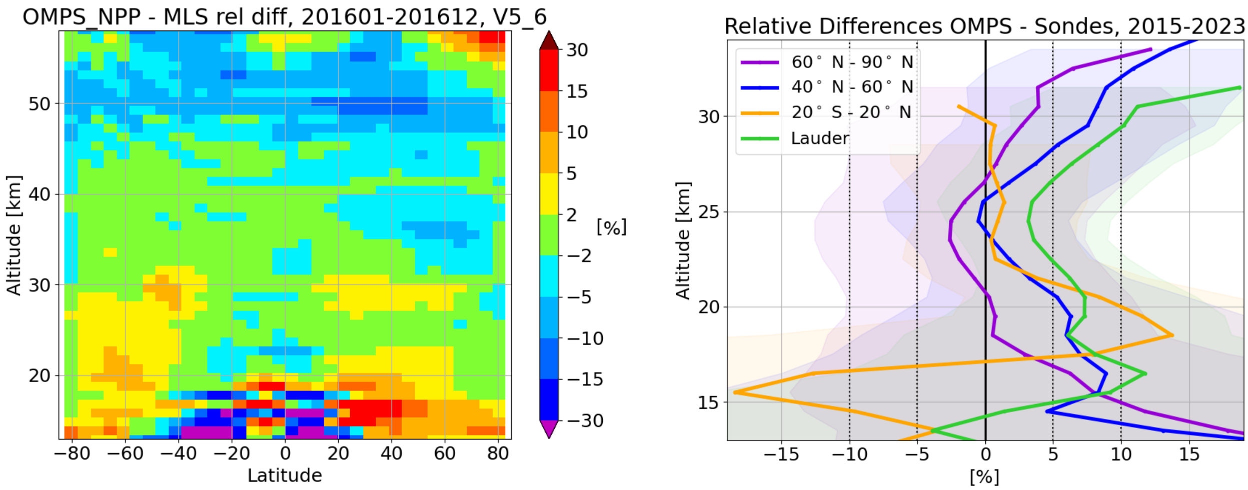

Figure 7. Left panel: relative difference between the collocated OMPS-LP and MLS profiles averaged over 2016. Right panel: relative difference between the collocated OMPS-LP and ozonesonde profiles averaged over 2012-2024

Overall there is good agreement with MLS within ±5 % between 20 and 50 km. Negative differences of about 10 % are seen in the upper part of the profiles. In the lower stratosphere-upper troposphere (UTLS) region, discrepancies of about 10 - 15 % are observed, which are generally negative in the tropics and positive at middle and high latitudes. The positive bias, which is more evident in the Northern hemisphere, is related to a positive bias of the VIIRS surface albedo with respect to that retrieved from OMPS-LP, when using the standard 1D retrieval. Furthermore, this discrepancy might also be caused by the uncertainty in the aerosol information used in ozone retrievals, which has the strongest impact in the Northern hemisphere. The results shown here are comparable to the validation results of the standard IUP retrieval, see e.g. Arosio et al. (2018), or to NASA results (Kramarova et al., 2024). This gives us confidence in the good quality of the produced 2D-mode dataset.

For comparisons with ozonesondes, we used the homogenized data from the HEGIFTOM project (Van Malderen and Smit, 2020; Van Malderen et al., 2025). To account for the very different vertical resolution, ozonesonde profiles were averaged over the vertical range corresponding to the typical vertical resolution of OMPS-LP profiles. We prefer not to use averaging kernels for this purpose for two reasons: (i) in the 2D-mode, the retrieval range is cut at the cloud top height and no averaging kernels are produced below, thus the averaging kernels for several lowermost layers are incomplete and no reliable results can

https://doi.org/10.5194/egusphere-2026-5113
Preprint. Discussion started: 4 September 2026

be produced for these layers; (ii) our previous studies have shown that the vertical averaging of the profiles and a smoothing with averaging kernels produce similar results for OMPS-LP ozone retrievals (Arosio et al., 2018). The relative differences between the OMPS-LP profiles and collocated ozonesonde data for 3 latitude bands and at the Lauder station are shown in the right panel of Fig. 7. Between 15 and 30 km, the discrepancies are generally within 10 %, except in the tropics where, due to the low ozone values, the relative differences are larger. Also for ozonesonde comparisons we see larger positive bias at northern high latitudes below 15 km.

Figure 8 shows the difference in SOC between collocated OMPS-LP and MLS observations, averaged over 1 year (2016), for the standard 1D-mode and for the 2D-mode retrievals. With respect to MLS, OMPS-LP generally reports larger SOC in the extra-tropics and slightly smaller SOC in the tropics (5 DU corresponds to about 2 % of the column). Results are comparable between the two versions, with a generally smaller bias of the 2D-mode version at southern mid-latitudes. The impact of the surface albedo bias mentioned in Sect. 5 is not very relevant in terms of SOC, slightly affecting, however, the difference with respect to MLS as a function of latitude. In summary, the new SOC agrees as a function of latitudes somewhat better with those from MLS. However there remain some differences which need to be further investigated.

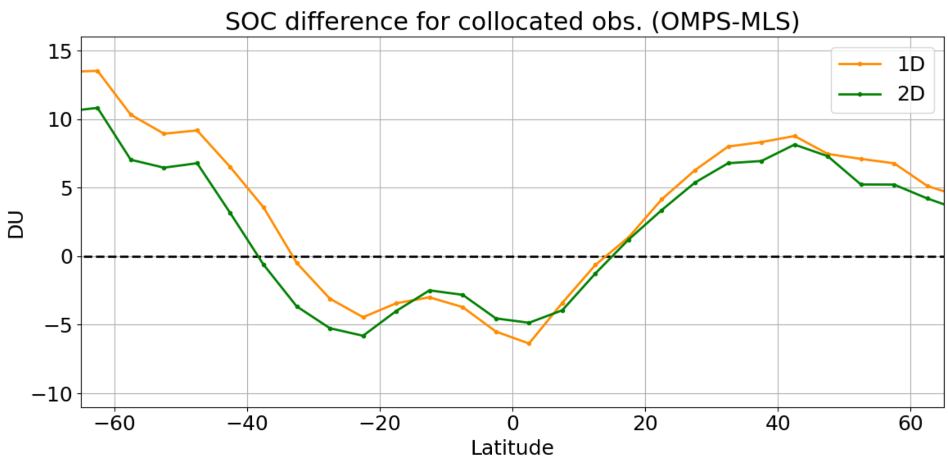

Figure 8. Zonal mean difference between the SOC from MLS and OMPS-LP for the 1D and 2D-mode retrievals.

https://doi.org/10.5194/egusphere-2026-5113
Preprint. Discussion started: 4 September 2026

7 Limb-Nadir matching and tropospheric ozone results

The new OMPS-LP 2D-mode stratospheric ozone dataset has been used to produce LNM TrOC data as discussed in this section. In particular, two datasets have been generated by combining 2D-mode SOC with OMPS-NM and TROPOMI total column observations. Both datasets provide valuable data between 60° N and S.

The first version of OMPS LNM dataset (v2.0), as mentioned in the introduction, was presented by Orfanoz-Cheuquelaf et al. (2024), combining IUP 1D limb retrievals (v3.3) and nadir observations from OMPS-NM. The validation presented in that paper shows that OMPS-LNM TrOC is generally slightly lower than the other datasets. The average bias with respect to ozonesondes was found to be -1.7 DU without significant latitudinal dependence.

Within the present work, this dataset has been re-processed and extended using the stratospheric ozone profiles from the 2D-mode retrieval. The overall methodology was not changed, the collocation criteria between limb and nadir observations and the ozone climatology used to extend limb profiles down to the tropopause remain the same (see Orfanoz-Cheuquelaf et al. (2024) for details). The TrOC are computed up to the blended tropopause, which is defined as follows: in the tropics, between 20° N and 20° S, the thermal tropopause is used, beyond 30° latitude, a dynamical tropopause with 3.5 PVU threshold is employed, and in the transition zone, between 20 and 30° latitude, the TPH is obtained as average of the thermal and dynamical tropopauses, weighted with the distance to the regime boundaries.

In Fig. 9 we compare the TrOC results obtained with the standard 1D and 2D-mode retrievals, i.e. v4.5 and v5.6, respectively, of the stratospheric profiles. TrOC was calculated using the same total ozone column (TOC) for both SOC datasets. In the top and middle panels of the plot, we observe a typical tropospheric ozone distribution with a maximum off-coast of western Africa, due to the production and transport of ozone precursors, significantly lower pollution in the tropical Pacific region, and strongly decreased TrOC values towards the southern high latitudes. In the bottom panel, we note that the differences between the two datasets are concentrated in specific locations, most prominently, in the Pacific band, to the South of Sahara desert, in the southern Mediterranean Sea, and to the South of the Arabian Peninsula. In all these regions, sharp gradients of the effective reflectance of the underlying scene are present along the LOS of OMPS-LP. These gradients are due to transitions from the ocean to the continent surface or from semi-stationary cloud bands to cloud-free scenes over the ocean. The sign of the changes depends on the direction of the albedo gradient. On top of these regional differences, that actually illustrate the effectiveness of the 2D-mode retrieval, we notice an overall negative bias in the southern middle and high latitudes.

In addition to the OMPS LNM TrOC product, we developed the TROPOMI-OMPS LNM dataset that combines TROPOMI TOC results from ESA and OMPS-LP SOC from IUP Bremen. As a result of the TROPOMI high spatial resolution, nearly all OMPS-LP ozone profiles have collocated TROPOMI measurements. As a consequence, we simply averaged all collocated TROPOMI pixels within ±1° latitude and ±0.5° longitude around each OMPS-LP measurement. Similarly to the OMPS LNM product, the SOC was calculated by integrating the limb ozone profiles down to the blended tropopause height. A climatology was used if the stratospheric profile bottom was above the tropopause.

https://doi.org/10.5194/egusphere-2026-5113
Preprint. Discussion started: 4 September 2026

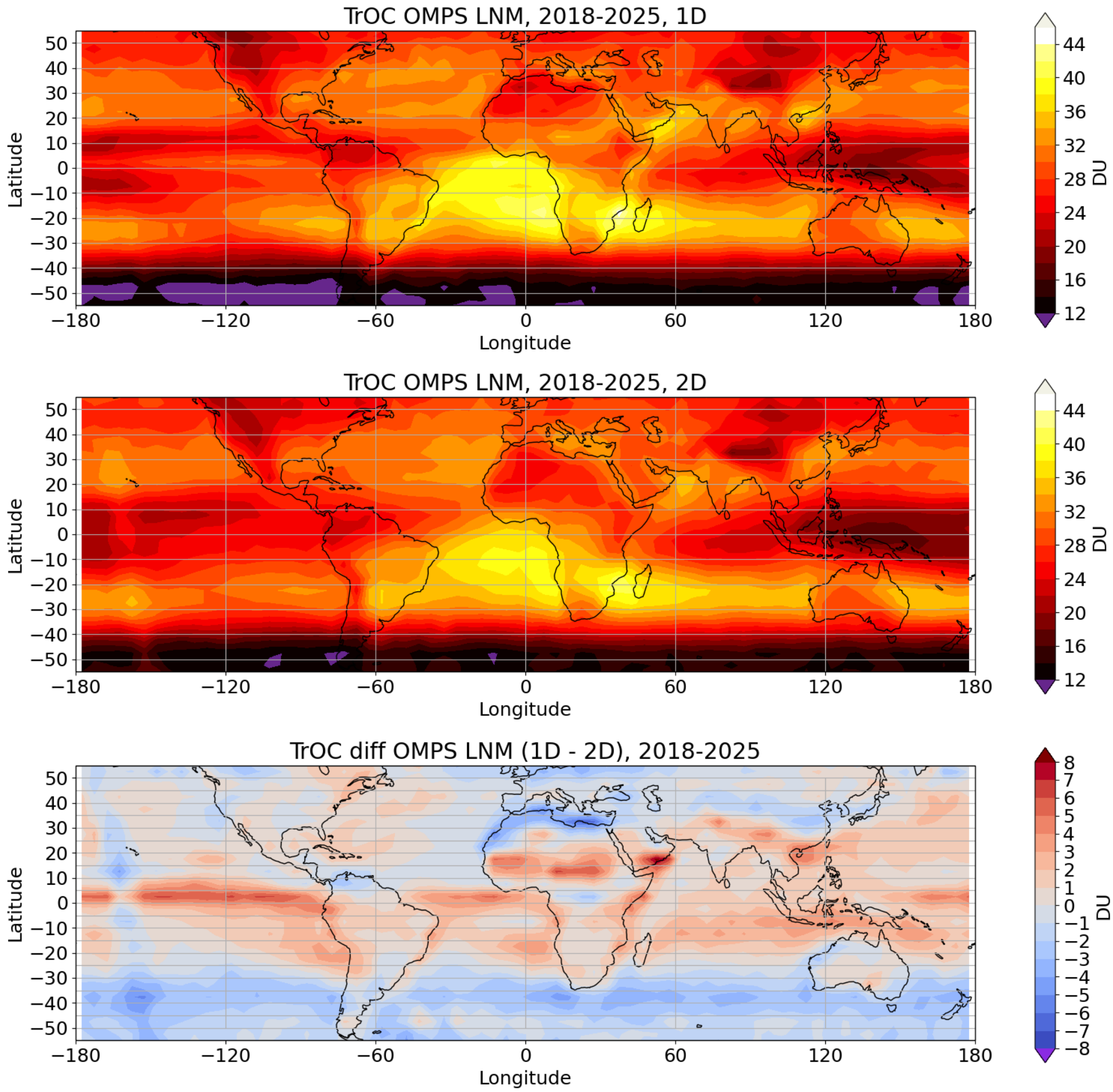

Figure 9. Multi-year mean TrOC obtained using 1D (top panel) and 2D-mode (middle panel) SOC and their difference (bottom panel).

Figure 10 shows the absolute difference between TROPOMI-OMPS LNM and OMPS LNM products, both obtained using 2D-mode retrieved SOC, averaged over the common 2018-2025 period. We notice an overall positive bias, i.e., TROPOMI-OMPS LNM results are 2-4 DU higher than those from OMPS LNM at most latitudes, except at northern mid-latitudes, where a small negative bias is seen in some regions.

https://doi.org/10.5194/egusphere-2026-5113
Preprint. Discussion started: 4 September 2026

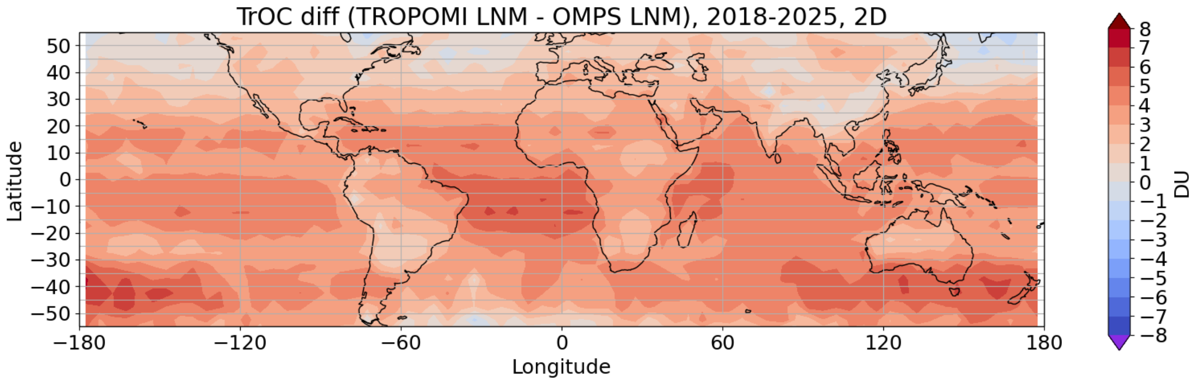

Figure 10. Absolute difference between TROPOMI-OMPS LNM and OMPS LNM products, averaged over 2018-2025.

To validate the new OMPS and TROPOMI-OMPS LNM datasets, we compared our results to the monthly averaged integrated HEGIFTOM ozonesonde profiles and to the tropospheric ozone columns from the OMI-MLS dataset (Ziemke et al., 2006), which provides global measurements of tropospheric ozone by combining data from OMI and MLS, both on board the Aura satellite. The OMI-MLS TrOC dataset provides monthly L3 data from 60° S to 60° N at a resolution of 5° latitude by 5° longitude. These data span the time from October 2004 to the present and were used in several studies to investigate long-term trends, pollution events and interactions with other atmospheric gases (Ziemke et al., 2019, 2022). Figure 11 shows two examples of TrOC time series from HEGIFTOM ozonesondes, OMI-MLS, OMPS LNM and TROPOMI-OMPS LNM (2D). We note an overall good agreement between the results, with mean discrepancies within 2-3 DU and a well reproduced seasonal behaviour by both LNM products. The latter are somewhat more noisy, especially OMPS LNM showing some visible outliers.

A general overview of the validation results is presented in Fig. 12. The plot shows mean differences and corresponding standard deviations with respect to the ozonesonde data for OMI-MLS, OMPS LNM (2D) and TROPOMI-OMPS LNM (2D) for all considered ozonesonde stations. In the tropics, both OMPS LNM and OMI-MLS show a very good agreement with ozonesondes while TROPOMI-OMPS LNM TrOC are generally a few DU higher. In the northern extra-tropics, we notice that both LNM products of IUP Bremen are generally low biased with respect to both ozonesondes and OMI-MLS. This was expected considering the positive bias of OMPS-LP ozone profiles with respect to MLS data, see Fig. 7, resulting in larger SOC and smaller TrOC. In the Northern Hemisphere, TROPOMI-OMPS LNM tends to provide a closer to zero mean deviation with respect to ozonesondes than OMPS LNM.

https://doi.org/10.5194/egusphere-2026-5113
Preprint. Discussion started: 4 September 2026

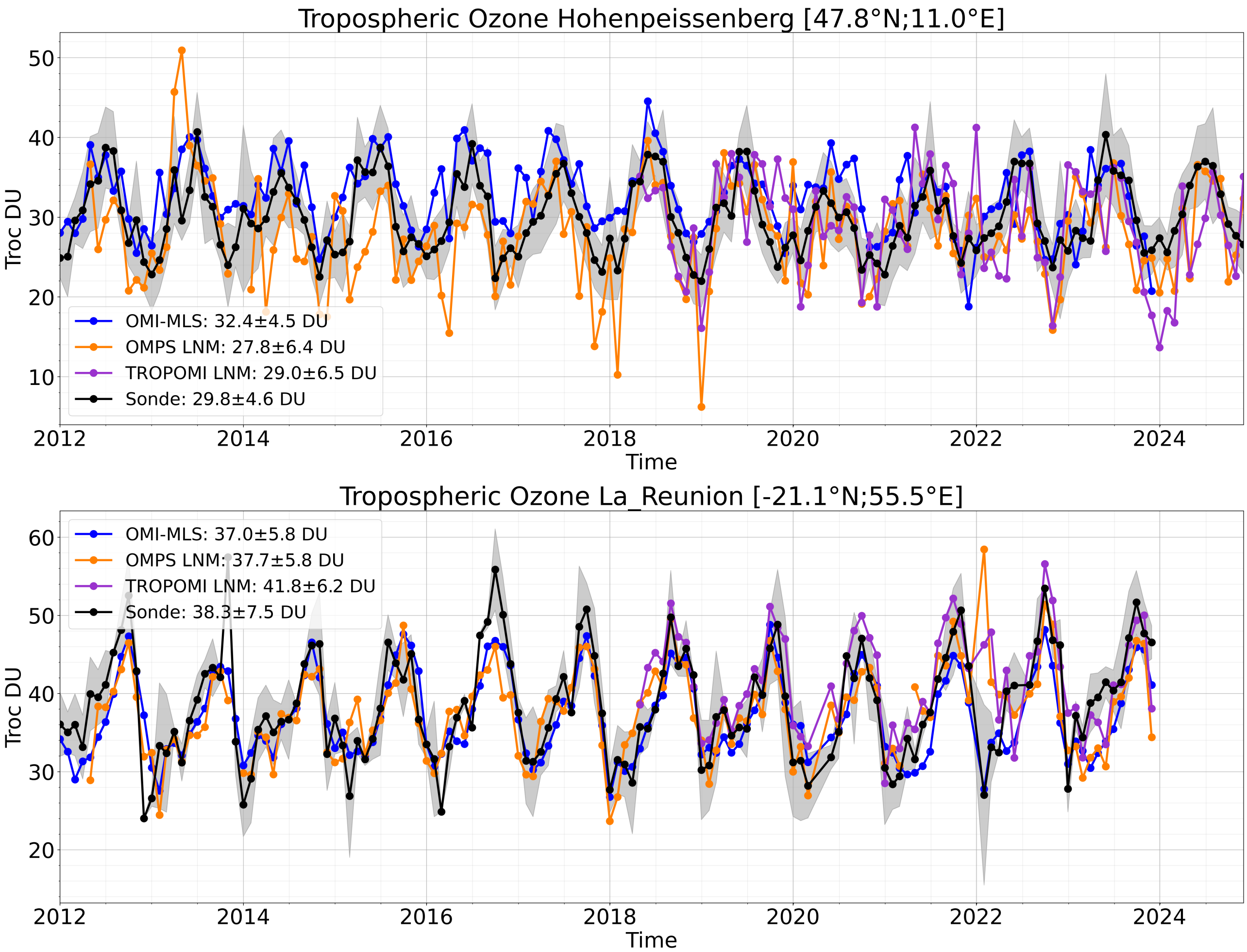

Figure 11. Time series of OMI-MLS, OMPS LNM, TROPOMI-OMPS LNM and integrated ozonesondes TrOC data at the two stations, Hohenpeissenberg and La Reunion.

8 Conclusions

In this study, we investigated the impact of the inhomogeneities of the underlying scene reflectance along the instrument LOS in the retrieval of stratospheric ozone profiles from limb measurements in the UV-Vis spectral range. The artifact resulting from these inhomogeneities is a general problem in the retrieval of ozone profiles from measured limb scans of solar-scattered radiation. The effect is particularly pronounced when the scene below the limb line of sight changes from a dark surface, such as the ocean, to a bright scene, for example above clouds. However, a bias can be introduced for all scenes below the limb line of sight if this contribution is not properly accounted for.

https://doi.org/10.5194/egusphere-2026-5113
Preprint. Discussion started: 4 September 2026

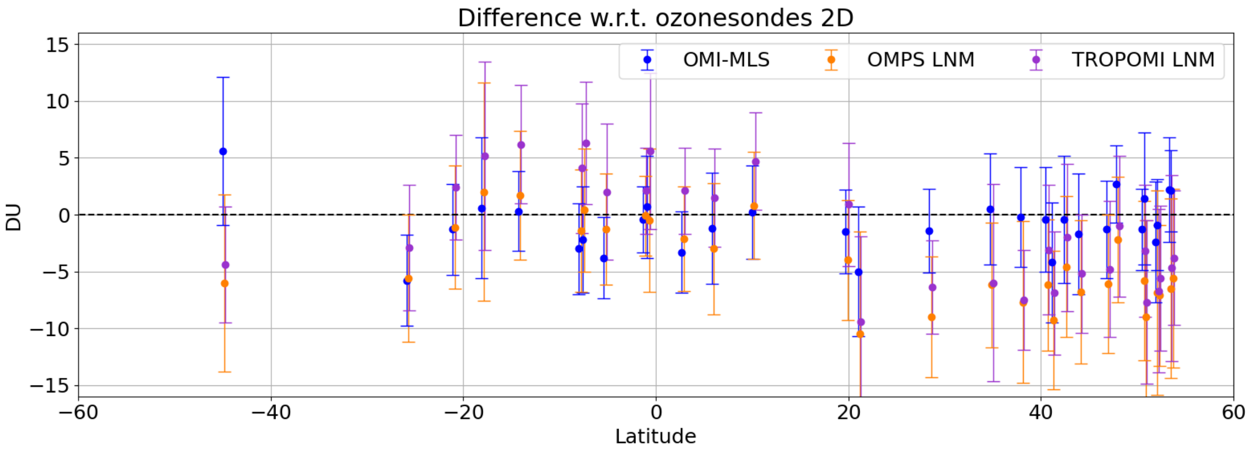

Figure 12. Mean differences with corresponding standard deviation between three LNM TrOC dataset and sondes, averaged over the 2018-2025 period.

An approach to account for this bias was developed by extending the forward RTM, SCIATRAN, to account for gradients in the effective Lambertian surface albedo along the instrument LOS. To initialize the SCIATRAN RTM, the along-orbit measurements of the effective Lambertian surface albedo from the VIIRS instrument were used. In the presented set-up, the albedo is only at a single wavelength in the visible range: a further step, which could bring an additional improvement of the product, is the usage of spectrally resolved information. Employing the newly developed retrieval approach, we processed the whole OMPS-LP time series (2012-2025) and updated/produced two LNM TrOC datasets: OMPS LNM and TROPOMI-OMPS LNM. Stratospheric profiles and TrOC datasets were compared against reference products and with the results from the standard retrieval. The comparison results demonstrated a successful mitigation of the artifacts in ozone related to inhomogeneities of the underlying scene reflectance along the instrument LOS, and an overall good agreement with the reference data for both stratospheric profiles and the TrOC products. An additional issue identified in this work is related to the uncertainty of the aerosol information used in the ozone retrieval. The latter seems to be responsible for a slight overestimation of ozone values in the lower stratosphere, particularly in the Northern hemisphere, which causes, as a consequence, a low bias in the LNM TrOC. Further investigations are needed to address this issue.

The research results presented here are important for the retrieval of ozone profiles from UV–Vis limb observations, including observations from SCIAMACHY and OSIRIS, as well as the upcoming ALTIUS mission. Correcting for this effect is relevant if such measurements are to provide the accuracy, stability and consistency required for long-term trend analyses, in line with the objectives and requirements of the Global Climate Observing System (GCOS) (Global Climate Observing System, 2022).

https://doi.org/10.5194/egusphere-2026-5113
Preprint. Discussion started: 4 September 2026

Data availability. The datasets produced at IUP and presented in this manuscript are available at https://www.iup.uni-bremen.de/DataRequest/. OMPS-LP Level 1 (v2.6) and Level 3 daily surface reflectance VIIRS (CMG V002) data are available at https://search.earthdata.nasa.gov/. The OMI-MLS tropospheric ozone dataset can be found at https://acd-ext.gsfc.nasa.gov/Data_services/cloud_slice/. TROPOMI Level 2 data used for the production of the LNM dataset are available at https://dataspace.copernicus.eu/

Author contributions. CA performed the testing of SCIATRAN 2D-mode, the processing of the OMPS ozone profiles and of the LNM datasets and wrote the manuscript draft. AR led the project and performed with VR the extension of the SCIATRAN RTM. AOC performed preliminary investigations and the retrieval of the original OMPS-NM data. HB, JPB and EM supervised the project. All co-authors contributed to the review of the manuscript. The identification of the issue addressed in this study and the recognition of the need to address it was developed by those authors involved in the SCIAMACHY project.

Competing interests. The authors declare that they do not have any competing interest.

Acknowledgements. This study has been primarily funded by ESA within the ENFORCE (Effect of Inhomogeneities in the Surface Reflectivity on Tropospheric Ozone Columns Retrieved by Using the Limb-Nadir Matching Technique) project, and by the State and University of Bremen. We would like to acknowledge the NASA team for the provided OMPS-LP data and for their support, as well as for producing consistent high-quality MLS and VIIRS datasets. Some of the ozonesonde data used in this publication are part of the Network for the Detection of Atmospheric Composition Change (NDACC) and are available through the NDACC website www.ndacc.org. We also acknowledge the data providers within SHADOZ and WOUDC networks. The processing of OMPS-LP stratospheric ozone and aerosol data has been done using the National High Performance Computing (NHR) infrastructure. The authors gratefully acknowledge the computing time granted by the Resource Allocation Board and provided for the supercomputers Lise and Emmy at NHR@ZIB and NHR@Göttingen. The calculations for this research were conducted using computing resources under projects no. hbk00062 and hbk00098. The OMPS-NM TOC retrievals were done using the HPC facilities of the IUP, University of Bremen, funded by DFG/FUGG grant nos. INST 144/379-1 and INST 144/493-1.

https://doi.org/10.5194/egusphere-2026-5113
Preprint. Discussion started: 4 September 2026

References

Arosio, C., Rozanov, A., Malinina, E., Eichmann, K.-U., von Clarmann, T., and Burrows, J. P.: Retrieval of ozone profiles from OMPS limb scattering observations, Atmospheric Measurement Techniques, 11, 2135–2149, 2018.

Arosio, C., Chipperfield, M., Rozanov, A., Weber, M., Dhomse, S., Feng, W., Jaross, G., Zhou, X., and Burrows, J.: Investigating zonal asymmetries in stratospheric ozone trends from satellite limb observations and a chemical transport model, Journal of Geophysical Research: Atmospheres, 129, e2023JD040 353, 2024.

Burrows, J., Hölzle, E., Goede, A., Visser, H., and Fricke, W.: SCIAMACHY—scanning imaging absorption spectrometer for atmospheric chartography, Acta Astronautica, 35, 445–451, https://doi.org/10.1016/0094-5765(94)00278-T, 1995.

Cao, C., Xiong, J., Blonski, S., Liu, Q., Uprety, S., Shao, X., Bai, Y., and Weng, F.: Suomi NPP VIIRS sensor data record verification, validation, and long-term performance monitoring, Journal of Geophysical Research: Atmospheres, 118, 11–664, 2013.

Crutzen, P. J., Lawrence, M. G., and Pöschl, U.: On the background photochemistry of tropospheric ozone, Tellus B: Chemical and Physical Meteorology, 51, 123–146, 1999.

Flittner, D. E., Bhartia, P. K., and Herman, B. M.: O3 profiles retrieved from limb scatter measurements: Theory, Geophysical Research Letters, 27, 2601–2604, https://doi.org/https://doi.org/10.1029/1999GL011343, 2000.

Flynn, L., Long, C., Wu, X., Evans, R., Beck, C., Petropavlovskikh, I., McConville, G., Yu, W., Zhang, Z., Niu, J., et al.: Performance of the ozone mapping and profiler suite (OMPS) products, Journal of Geophysical Research: Atmospheres, 119, 6181–6195, 2014.

Global Climate Observing System: The 2022 GCOS ECVs Requirements, Report GCOS-245, World Meteorological Organization, Geneva, 2022.

Heue, K.-P., Coldewey-Egbers, M., Delcloo, A., Lerot, C., Loyola, D., Valks, P., and Van Roozendael, M.: Trends of tropical tropospheric ozone from twenty years of European satellite measurements and perspectives for Sentinel-5 Precursor, Atmospheric Measurement Techniques Discussions, 2016, 1–21, 2016.

Hwang, Y. and Frierson, D.: A new look at the double ITCZ problem: Connections to cloud bias over the Southern Ocean, Proc. Natl Acad. Sci. USA, 110, 4935–4940, 2013.

Keppens, A., Di Pede, S., Hubert, D., Lambert, J.-C., Veefkind, P., Sneep, M., De Haan, J., Ter Linden, M., Leblanc, T., Compernolle, S., et al.: Five years of Sentinel-5p TROPOMI operational ozone profiling and geophysical validation using ozonesonde and lidar ground-based networks, Atmospheric Measurement Techniques Discussions, 2024, 1–43, 2024.

Kramarova, N. A., Xu, P., Mok, J., Bhartia, P., Jaross, G., Moy, L., Chen, Z., Frith, S., DeLand, M., Kahn, D., et al.: Decade-long ozone profile record from Suomi NPP OMPS Limb Profiler: Assessment of version 2.6 data, Earth and Space Science, 11, e2024EA003 707, 2024.

Leventidou, E., Eichmann, K.-U., Weber, M., and Burrows, J. P.: Tropical tropospheric ozone columns from nadir retrievals of GOME-1/ERS-2, SCIAMACHY/Envisat, and GOME-2/MetOp-A (1996–2012), Atmospheric Measurement Techniques, 9, 3407–3427, 2016.

Livesey, N. J., Van Snyder, W., Read, W. G., and Wagner, P. A.: Retrieval algorithms for the EOS Microwave limb sounder (MLS), IEEE Transactions on Geoscience and Remote Sensing, 44, 1144–1155, 2006.

Mettig, N., Weber, M., Rozanov, A., Burrows, J. P., Veefkind, P., Thompson, A. M., Stauffer, R. M., Leblanc, T., Ancellet, G., Newchurch, M. J., et al.: Combined UV and IR ozone profile retrieval from TROPOMI and CrIS measurements, Atmospheric Measurement Techniques, 15, 2955–2978, 2022.

Oikarinen, Liisa, E. S. and Kyrölä, E.: Multiple scattering radiance in limb-viewing geometry, Journal of Geophysical Research: Atmospheres, 104, 31 261–31 274, https://doi.org/https://doi.org/10.1029/1999JD900969, 1999.

Oikarinen, L.: Effect of surface albedo variations on UV-visible limb-scattering measurements of the atmosphere, Journal of Geophysical Research: Atmospheres, 107, ACH–13, 2002.

Orfanoz-Cheuquelaf, A., Rozanov, A., Weber, M., Arosio, C., Ladstätter-Weißenmayer, A., and Burrows, J. P.: Total ozone column from Ozone Mapping and Profiler Suite Nadir Mapper (OMPS-NM) measurements using the broadband weighting function fitting approach (WFFA), Atmospheric Measurement Techniques, 14, 5771–5789, 2021.

Orfanoz-Cheuquelaf, A., Arosio, C., Rozanov, A., Weber, M., Ladstätter-Weißenmayer, A., Burrows, J. P., Thompson, A. M., Stauffer, R. M., and Kollonige, D. E.: Tropospheric ozone column dataset from OMPS-LP/OMPS-NM limb–nadir matching, Atmospheric Measurement Techniques, 17, 1791–1809, 2024.

Rozanov, A., Rozanov, V., and Burrows, J. P.: A numerical radiative transfer model for a spherical planetary atmosphere: Combined differential–integral approach involving the Picard iterative approximation, Journal of Quantitative Spectroscopy and Radiative Transfer, 69, 491–512, 2001.

Rozanov, V., Rozanov, A., Kokhanovsky, A., and Burrows, J.: Radiative transfer through terrestrial atmosphere and ocean: software package SCIATRAN, Journal of Quantitative Spectroscopy and Radiative Transfer, 133, 13–71, 2014.

Steck, T., Höpfner, M., von Clarmann, T., and Grabowski, U.: Tomographic retrieval of atmospheric parameters from infrared limb emission observations, Applied optics, 44, 3291–3301, 2005.

Stevenson, D., Young, P., Naik, V., Lamarque, J.-F., Shindell, D. T., Voulgarakis, A., Skeie, R. B., Dalsoren, S. B., Myhre, G., Berntsen, T. K., et al.: Tropospheric ozone changes, radiative forcing and attribution to emissions in the Atmospheric Chemistry and Climate Model Intercomparison Project (ACCMIP), Atmospheric Chemistry and Physics, 13, 3063–3085, 2013.

Van Malderen, R. and Smit, H. G. J.: HEGIFTOM webpage, https://hegiftom.meteo.be/, accessed: 2024-11-21, 2020.

Van Malderen, R., Zang, Z., Chang, K.-L., Björklund, R., Cooper, O. R., Liu, J., Barras, E. M., Vigouroux, C., Petropavlovskikh, I., Leblanc, T., Thouret, V., Wolff, P., Effertz, P., Gaudel, A., Tarasick, D. W., Smit, H. G., Thompson, A. M., Stauffer, R. M., Kollonige, D. E., Poyraz, D., Ancellet, G., de Backer, M.-R., Frey, M. M., Hannigan, J. W., Hernandez, J. L., Johnson, B. J., Jones, N., Kivi, R., Mahieu, E., Morino, I., Mcconville, G., Müller, K., Murata, I., Notholt, J., Piters, A., Prignon, M., Querel, R., Rizi, V., Smale, D., Steinbrecht, W., Strong, K., and Sussmann, R.: Ground-based Tropospheric Ozone Measurements: Regional tropospheric ozone column trends from the TOAR-II/HEGIFTOM homogenized datasets, Atmospheric Chemistry and Physics, 2025.

Veefkind, J. P., Aben, I., McMullan, K., Förster, H., De Vries, J., Otter, G., Claas, J., Eskes, H., De Haan, J., Kleipool, Q., et al.: TROPOMI on the ESA Sentinel-5 Precursor: A GMES mission for global observations of the atmospheric composition for climate, air quality and ozone layer applications, Remote sensing of environment, 120, 70–83, 2012.

Veefkind, P., Kleipool, Q., Ludewig, A., Aben, I., Dehn, A., Loyola, D., Nett, H., Richter, A., van Roozendael, M., Siddans, R., et al.: Overview of Early Results from TROPOMI on the Copernicus Sentinel 5 Precursor, in: EGU General Assembly Conference Abstracts, p. 12216, 2018.

Zawada, D. J., Rieger, L. A., Bourassa, A. E., and Degenstein, D. A.: Tomographic retrievals of ozone with the OMPS Limb Profiler: algorithm description and preliminary results, Atmospheric Measurement Techniques, 11, 2375–2393, 2018.

Ziemke, J., Chandra, S., and Bhartia, P.: A 25-year data record of atmospheric ozone in the Pacific from Total Ozone Mapping Spectrometer (TOMS) cloud slicing: Implications for ozone trends in the stratosphere and troposphere, Journal of Geophysical Research: Atmospheres, 110, 2005.

https://doi.org/10.5194/egusphere-2026-5113
Preprint. Discussion started: 4 September 2026

Ziemke, J., Chandra, S., Duncan, B., Froidevaux, L., Bhartia, P., Levelt, P., and Waters, J.: Tropospheric ozone determined from Aura OMI and MLS: Evaluation of measurements and comparison with the Global Modeling Initiative's Chemical Transport Model, Journal of Geophysical Research: Atmospheres, 111, 2006.

Ziemke, J. R., Oman, L. D., Strode, S. A., Douglass, A. R., Olsen, M. A., McPeters, R. D., Bhartia, P. K., Froidevaux, L., Labow, G. J., Witte, J. C., Thompson, A. M., Haffner, D. P., Kramarova, N. A., Frith, S. M., Huang, L.-K., Jaross, G. R., Seftor, C. J., Deland, M. T., and Taylor, S. L.: Trends in global tropospheric ozone inferred from a composite record of TOMS/OMI/MLS/OMPS satellite measurements and the MERRA-2 GMI simulation, Atmospheric Chemistry and Physics, 19, 3257–3269, 2019.

Ziemke, J. R., Kramarova, N. A., Frith, S. M., Huang, L.-K., Haffner, D. P., Wargan, K., Lamsal, L. N., Labow, G. J., McPeters, R. D., and Bhartia, P. K.: NASA Satellite Measurements Show Global-Scale Reductions in Free Tropospheric Ozone in 2020 and Again in 2021 During COVID-19, Geophysical Research Letters, 49, e2022GL098 712, 2022.